# Carbon nanotube thin film transistors by droplet electrophoresis

Lefebvre, J.; Ding, J.



**Publisher's version / Version de l'éditeur:**
https://doi.org/10.1016/j.mtcomm.2017.01.002
*Materials Today Communications, 10, pp. 72-79, 2017-01-17*

Materials Today Communications 10 (2017) 72–79

Contents lists available at ScienceDirect

Materials Today Communications

journal homepage: www.elsevier.com/locate/mtcomm

# Carbon nanotube thin film transistors by droplet electrophoresis

J. Lefebvre*, J. Ding

*National Research Council, 1200 Montreal Road, Ottawa, ON, K1A 0R6, Canada*

ARTICLE INFO

*Article history:*
Received 1 November 2016
Received in revised form 5 January 2017
Accepted 6 January 2017
Available online 17 January 2017

ABSTRACT

Spontaneously charged aerosol droplets, each containing a few single-walled carbon nanotubes wrapped in conjugated polymers were precipitated on a target substrate using electrostatic forces. Nanotube networks were assembled on a variety of dielectric surfaces including polymers with low surface energy: Good transistor performance was achieved in all cases. Under proper regime of electrostatic and flow fields, patterns were produced in a maskless fashion and feature sizes below 150 μm were demonstrated.


## 1. Introduction

With its of ease of fabrication combined with performance, thin films of randomly organized carbon nanotubes (mainly single-walled –SWCNT-) have attracted a lot of interest in conductive and transistor applications [1–3]. The methods to obtain such films are more or less sophisticated depending on the end goal: From dry transfer and soaking to self-assembly; [4–9] Or from spraying to inkjet or aerosol jet printing [10–19]. For SWCNT based transistors in printed electronics, requirements on the film morphology are quite stringent if mobility in excess of 10 $cm^2$/Vs is to be achieved while maintaining a low *Off-state* current. Moreover, a suitable deposition method should allow for patterns with 10–100 μm resolution with good uniformity across macroscopic areas, as well as scalability and throughput as primary considerations. The present work was motivated by the limited number of printing methods capable of achieving these requirements.

In order to explore new territories, we asked the question whether it would be possible to efficiently deliver carbon nanotubes a few at a time to a target surface. In the formation of a random network, this situation would appear ideal since individual droplets containing one or a few nanotubes would evaporate independently of one another: Bundling/coffee staining would be minimized. Common printing methods operate away from this regime with concentrated carbon nanotube solutions being used. Those methods rely on efficient spread of material to achieve desired film morphologies.

Aerosol generation provides unexplored opportunities for carbon nanotube network and thin film assembly. With sub-micron droplet generators commercially available, the few nanotube regime is reached with reasonable carbon nanotube concentrations. For example, with 1–2 μm diameter droplets (1–4 fL), a single nanotube per droplet requires concentrations of order of 1 μg/mL, a modest 10–50x dilution compared to dispersions used by our group for inkjet printing [19]. The high throughput of aerosol generators, >$\mu L/s$, should be sufficient to cover $cm^2$ areas with 10–100 *nanotubes*/$\mu m^2$ in seconds. In addition to accessing a new dilution regime, a different flow regime for droplet delivery can be explored: Laminar. In contrast with aerosol jet printing, droplets can be carried at velocities of order of *cm/s*, more than hundred times slower. In this regime, external forces need to act on micro-droplets to promote the yield of deposited material; Otherwise droplets will be efficiently carried away from surfaces. Electrostatic forces represent a convenient choice: The field can act on droplets to counter the action of the laminar flow and move them to a target substrate.

In this paper, we demonstrate that sc-SWCNT thin film transistors with good performance can be assembled from electrophoretically transported micron-size droplets, each containing one or a few carbon nanotubes. Nanotube networks were assembled on a variety of dielectric surfaces including polymers with low surface energy where hysteresis-free transport is measured. We also demonstrate that under proper control of the gas flow and electric field, patterned deposition was achieved without use of a mask, with feature size below 150 μm.

## 2. Experimental

### 2.1. Single-walled carbon nanotube dispersion

The sc-SWCNTs dispersions were prepared from enriched plasma sc-SWCNTs (diameter around 1.3 nm), using a hybrid

* Corresponding author.
*E-mail address:* Jacques.lefebvre@nrc-cnrc.gc.ca (J. Lefebvre).

http://dx.doi.org/10.1016/j.mtcomm.2017.01.002

process previously reported by our group [20,21]. In brief, raw material from Raymor Nanotechnologies (RN-000) was mixed with poly(9,9-didodecylfluorene), PFDD in toluene at a polymer to SWCNT ratio of 1.0/1.0 and a nanotube concentration of 0.8 mg/mL. The mixture was horn sonicated for 30 min (Branson sonifier 250) followed by 30 min centrifugation (relative centrifuge force of ≈18,000*g*). This step was repeated 5 times using the sediment from the previous centrifugation and the five supernatant solutions were combined and added with silica gel at a usage of 1 mg/mL. The mixture was sonicated in a bath sonicator (Branson 2510) for 40 min, followed by standing for 3 h, and then 30 min centrifugation (relative centrifuge force of ~18,000*g*). The supernatant was filtered using a Teflon membrane with 0.2 μm pore size (Sartorus Stedim Biotech) and rinsed with toluene to remove excess polymer. The collected sc-SWCNTs were dispersed in toluene using bath sonication for 5–10 min at a concentration of 0.48 mg/mL and a polymer to nanotube weight ratio of 2.4. The >99.9% purity solution is dominated by SWCNT chiralities around *(10,9)* [20,22,23]. Transistors made from soaking on $SiO_2$/Si substrates show high mobility combined with high On/Off ratio (average nanotube length is 1.3 μm [20,24]). Prior to aerosol deposition, dilute solutions starting from a 480 μg/mL were prepared in 20–25 mL quantities by adding toluene and sonicating for 60 min in a Branson 1250.

### 2.2. Carbon nanotube deposition

The formation of a nanotube network is based on using electrostatic forces to attract charged aerosol droplets to a target substrate. An aerosol generator, 241 PG from Sonaer Inc., breaks a nanotube containing solution into micron-size droplets (calculated hydrodynamic diameter of 1.7 μm for water and 1.3 μm for toluene [25,26]. Measured values provided by Sonaer for water are: *Mass median dia.*: 3.7 μm; *Sauter mean dia.*: 2.9 μm; *Volume mean dia.*: 1.8 μm; *Area mean dia.*: 1.4 μm; *Number mean dia.*: 1.2 μm). Droplets are carried to a deposition chamber using a low flow rate $N_2$ gas (50–150 sccm in *¼ inch* Teflon tubing). They enter the chamber through a brass nozzle set to a high voltage (Standford Research PS350 for DC voltages and function generator/amplifier combo for AC voltages) with respect to the sample holder. Voltages in the 100–2500 V range have been applied. The distance between the nozzle and the sample is about 2 *mm* for the results presented here but larger gaps have been used. The chamber sits on a hot plate held at 75 °*C*; This temperature is sufficiently high to quickly evaporate droplets and sufficiently low to avoid thermal gradients and convection. Gases ($N_2$ and toluene) are exhausted through a $N_2$ cold trap to collect residual particles before being vented to a hood.

### 2.3. Transistor fabrication

Substrates were $SiO_2$/Si with the doped Si acting as a common backgate electrode and $SiO_2$ as the gate dielectric (100 nm). Wafers were limitedly cleaned, with only a 30 min exposure to UV-$O_3$. Samples produced in the aerosol process were initially insulating. Even a small amount of excess polymer (2.5:1 weight ratio with respect to SWCNT) was sufficient to prevent conduction and a rinsing step was required. Soon after the deposition step, samples were bathed in toluene for 5 min followed by isopropanol and dried with $N_2$ gas. Optical absorption obtained from thoroughly rinsed dispersions have polymer:nanotube weight ratio of 1 or slightly less. A 5–10 min bake at 150 °C was also performed, for consistency with our soaking process. Source-drain contacts (Ti/Au) were evaporated through a shadow mask (Tecan, UK) to produce transistors with dimensions from $12 \times 220$, $20 \times 220$ and $40 \times 220\ \mu m^2$. At those length scales, current scales with channel length and was not limited by contact resistance. A photo of the sample used in Fig. 3 is shown in Fig. S5. Samples fabricated on polymer dielectrics have been described in Ref. [27].

### 2.4. Thin film characterization (optical, SEM, Raman, electrical)

#### 2.4.1. Optical

Macro-photography pictures taken under different illumination conditions are presented throughout this manuscript. Since the films are ultrathin, special attention was given to illumination conditions. A powerful fibre illuminator source worked best to reveal the film through scattered light. In some cases, fluorescence from the poly-fluorene was found useful, as well as light interference seen as angle dependent coloration changes on thin oxide layers. Several examples are presented in Figs. S4–S8. All photos were taken prior to the rinsing step after which the films were only visible to a well-trained eye.

#### 2.4.2. SEM

A Hitachi 4700 electron microscope was operated under optimum conditions to observe SWCNTs in charge contrast mode: 0.5–1 kV acceleration voltage and 4 mm working distance.

#### 2.4.3. Raman scattering

Both commercial and home-built Raman systems operating at 532 nm excitation wavelength were used for this work. This wavelength is resonant with higher optical transitions in sc-SWCNTs with diameters around 1.3 nm [23].

#### 2.4.4. Electrical testing

Transistor transfer characteristics (current versus gate bias) were acquired in air ambient using a home-built probe station (voltage source, ammeter, function generator and oscilloscope). The source-drain bias was set to 0.5 V and the current (Keithley 6517A) output fed to the input of a digital oscilloscope (Agilent DSO6012A). A 110 mHz saw tooth voltage from a function generator (Agilent 33220A) was applied to the backside of the sample (Si substrate covered with 100 nm thermal oxide or polymer dielectric). This voltage was also fed as input to the oscilloscope. Hole mobility was calculated from the slope of the transfer curves using the parallel plate capacitor model. Device configuration and dimensions are given in Fig. S6(e).

## 3. Results

### 3.1. Electrostatic precipitation

Fig. 1 summarizes the main findings. The setup, illustrated in Fig. 1(a) is in many ways similar to other aerosol processes (see Fig. S1 for photos of the setup): a particle generator turns a carbon nanotube dispersion into droplets. Here, we used a high frequency (2.4 MHz) ultrasonic generator to produce 1–2 μm diameter droplets. Generated droplets were transported to a deposition chamber using $N_2$ as carrier gas. A low flow rate ensures droplets were carried in a laminar fashion, with minimum droplet coalescence expected. Tubing was also kept very short to limit droplet evaporation: we estimate droplets should take only a few seconds to travel the total distance between the generator and the substrate. At the deposition chamber, tubing is connected to a nozzle with different configurations of aperture (single hole, many holes or slit aperture). Typical dimensions for slit openings were $\approx 0.5 \times 20\ mm^2$. Substrates were heated sufficiently to quickly evaporate the droplets. We expect that droplets evaporate mainly once they reach the substrate surface, since the time to cover the small distance between the nozzle and the substrate is very short ($\ll$1 s).

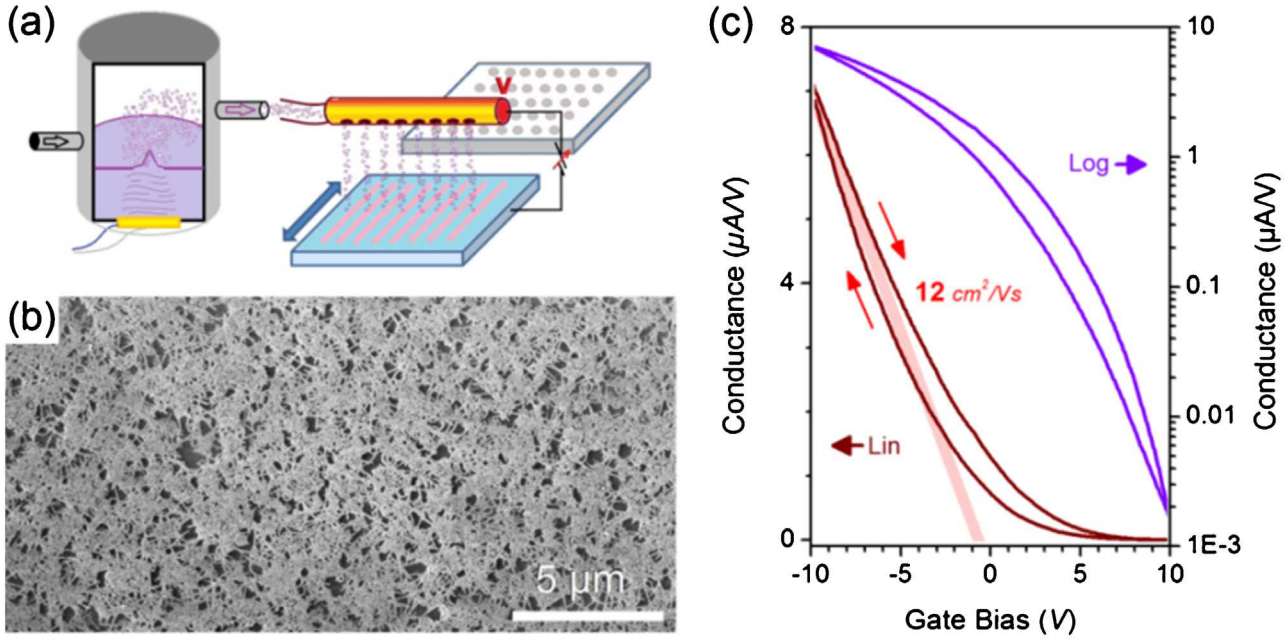


**Fig. 1.** Carbon nanotubes thin film by droplet precipitation. (a) Schematic illustration of the deposition system and process. Using a combination of nozzle (yellow-orange) aperture, electrostatic field and sample translation, patterned deposition is achieved. See Fig. S1 for several photographs of the experimental setup. (b) Scanning electron microscopy image of a network of SWCNTs. (c) Transistor characteristic for a sc-SWCNT thin film on $SiO_2$/Si (1000 nm oxide). Channel length and width are 12 and 220 μm, respectively. Mobility is calculated using the standard plate capacitor model. 7 μA/V is equivalent to 0.03 μA/μm for these devices.

The main attributes of the method is summarized in three points: 1–2 μm diameter charged droplets, each containing a few carbon nanotubes; A low flow rate to carry droplets in a laminar fashion; An electrostatic field to precipitate droplets on a substrate. The substrate can be a conductor or an insulator (thicknesses up to 150 μm have been tested). The nozzle can be a conductor connected to a voltage source or a tribo-statically charged insulator (for example Teflon rubbed with an aluminum foil). This paper focuses on solutions of polymer wrapped sc-SWCNTs in toluene but unsorted SWCNTs in chlorobenzene have also been tested, with qualitatively similar results with regards to film morphology.

Fig. 1(b) shows an SEM (scanning electron microscopy) example of a random network of SWCNTs on a $SiO_2$/Si substrate. In several ways, films resemble others made by soaking or drop casting and consist of a sparse assembly of ≈1 μm long nanotubes (average nanotube length is 1.3 μm [20]) with areal densities of order 10–50 $\mu m^{-2}$. In contrast with soaking, small areas with "missing" material are seen in the network at lower coverages; nanotubes are most often not straight but are slightly curved, a consequence of the nanotube conformation inside spherical droplets. Although SEM provides a good indication that the network morphology is suitable for thin film transistors, this is confirmed with electronic performance data. Fig. 1(c) presents a transfer curve from the best films achieved thus far: the hole field effect mobility is quite respectable at >10 $cm^2$/Vs and On/Off ratio in excess of 10,000. These values are lower than films obtained in our group by soaking or inkjet printing where mobility in excess of 30 $cm^2$/Vs has been achieved [19,20,24]. Recent work on networks of polymer wrapped sc-SWCNTs obtained by inkjet printing also showed good mobility (close to 10 $cm^2$/Vs) for both electrons and holes in a top gated transistor [18]. Here, several parameters have yet to be optimized and may account for the lower performance compared to other depositions methods explored in our group. The difference may also be intrinsic to the film morphology, where straighter nanotubes are seen for soaking and inkjet, with consequently fewer inter-nanotube junctions to bridge source-drain electrodes. Improvements in the film morphology is expected with larger droplets which can be controlled with the choice of aerosol generator or an optimized nanotube dispersion.

In terms of throughput, centimeter square areas are typically covered in a few minutes, even at the lowest concentrations presented here. At 1 μg/mL, it takes 5 μL of solution to cover a $cm^2$ with 100 *Nanotubes*/$\mu m^2$. We estimate that 1–2 mL is aerosolized per hour of operation using 241 PG generator. With 1 min being typical of a deposition run, ≈10–20 μL is therefore required for one run. The yield from this calculation is reasonably high at ≈25–50%. Later, we will show that collected droplets are spontaneously charged and this yield suggests that they represent a good fraction of generated droplets. If the number of neutral droplets was fairly high, the yield of deposited material would be much lower, unless dielectrophoretic forces were at play. Using external means to intentionally charged droplets should maximize process yield and throughput.

In addition to producing suitable nanotube networks on $SiO_2$ dielectric, good adhesion was found even on surfaces with very low surface energy. For example, bottom gate air exposed thin film transistors have been fabricated on several polymer dielectrics, including hydrophobic Teflon-AF and poly(vinyl phenol)/poly(methyl silsesquioxane) blend (PVP-pMSSQ) where gate hysteresis was greatly suppressed [27]. Results from six polymer dielectrics including Teflon-AF and PVP-pMSSQ are shown as supporting information (Fig. S2). We speculate that "*one at a time*" delivery of nanotubes in this aerosol method prevents significant reorganization of the network during and after its formation. Once formed, the collective arrangement of nanotubes cannot be easily disrupted, even in a rinsing step.

In terms of uniformity over macroscopic scales, mapping of transistor performance across an entire sample (Fig. S3) shows +/− 10% variability on the mobility within $mm^2$ areas. This number is likely limited only by the ability to properly engineer and control the delivery of aerosol to the surface. In any case, this paper wishes to highlight the unique attributes of this aerosol process: deposition in a few nanotube regime, electrostatic precipitation of droplets, and patterned maskless deposition under laminar flow

and electrostatic fields. Moreover, the method addresses an important challenge with printing carbon nanotube inks: adhesion on polymer surfaces. This is often mitigated by treating the surface using a plasma [18,19,28], a process which induces traps in the dielectric material and consequently degrades transistor performance. The aerosol process presented here allows for deposition on any surfaces, without any harsh surface pretreatment.

Fig. 2 highlights the critical role of electrostatic in the assembly of carbon nanotube networks by aerosol. For this and the majority of experiments presented here, a slit shape nozzle was used (Fig. S1). Fig. 2(a) (see Figs. S4–S5 for the complete dataset) shows a series of films deposited under increasingly higher voltages. Fig. 2(b-g) show corresponding SEM images. Under the action of an electrostatic field, an initially sparse network of carbon nanotubes is substituted with a dense mat of highly connected nanotubes. In absence of applied voltage (see Fig. S4(a)), a limited amount of material is found. Even at the very low flow rate of carrier gas (50 sccm $N_2$, which corresponds to a linear velocity around 1 cm/s for our geometry. *sccm* stands for standard cubic centimeter per minute), the micron size droplets are carried away from regions directly under the slit-shape nozzle and only a small amount ends up on the substrate. Upon applying a moderate voltage (±100 V in Fig. 2(b–c)), nanotube material starts to concentrate under the nozzle and the amount of deposited material is significantly increased compared to 0 V. Two lobes of material are apparent and they extend a few millimeters on both sides of the nozzle long axis. As the voltage is increased to ±400 V, the side lobes gradually disappear and material concentrates further and further under the nozzle. In Fig. 2(f–g), ±1600 V were applied and narrow stripes of material are being deposited. Qualitatively, the polarity of the applied voltage does not significantly influence material deposition. It is worth emphasizing that by the nature of the droplets, specifically their size and the number of nanotubes they contain, we have observed no evidence of coffee stain at the macro-scale.

In order to gain a greater physical insight of the process, we have performed Raman scattering measurements on the three samples in Fig. S4(a–c). In Fig. 2(h), the G-band intensity is plotted as a function of applied voltage, with intensity normalized to account for the varying duration between the three sample deposition times. The data shows a linear increase of deposited material up to ≈700 V followed by a sub-linear increase and saturation at high voltages. A very good symmetry is observed between positive and negative voltages, but with a slight asymmetry favoring higher coverages at positive voltages. Using the 0 and 2000 V data, close to a hundred-fold enhancement has been estimated.

### 3.2. Few nanotubes per droplet

The initial premise of this work was that the best network morphology should be achieved in a regime where nanotubes are deposited one by one. Using reasonable parameters that reflect our sc-SWCNT material (see Supporting Information under “ONE NANOTUBE per DROPLET”), we have calculated a cross-over concentration where each droplet should contain on average one nanotube or less. We then proceeded to assemble carbon nanotube networks using four dilutions, two below and two above 3 μg/mL, the cross-over value. The duration of the deposition was adjusted to obtain nominally the same amount of material. SEM micrographs are presented in Fig. 3(a–d). Starting with the highest dilution, 0.9 μg/mL, we find a network with excellent uniformity with individual nanotubes being slightly curled. As the concentration increases, clumping starts to become significant with several openings exposing the underlying $SiO_2$/Si substrate. For each dilution, images were also taken away from the nozzle area to reveal the morphology of individual droplets. At the highest concentration, 14.1 μg/mL, micro-coffee stains form with at least 10–12 nanotubes clumped together. As the concentration is reduced, individual droplets appear to contain fewer and fewer nanotubes and little evidence of micro-coffee stains can be found.

Raman measurements performed on this sample support our SEM observations. In order to reveal the effect of dilution, the intensity from 24 neighboring locations was averaged. Fig. 3(e) shows the average intensity and the standard deviation (as an error bar) for the four concentrations in this study (two deposition times were looked at to confirm the expected linearity). We first observe that the amount of material is essentially flat for the first two concentrations and then increases to almost double at 14.1 μg/mL. This result indicates stronger electrostatic forces when more nanotubes occupy a single droplet. At the same time, the standard deviation more than doubles indicating that uniformity worsens dramatically, consistent with SEM results. Both SEM and Raman data demonstrate that below 3 μg/mL, good network morphology is obtained: That regime corresponds to one or few carbon nanotubes being deposited for each droplet reaching the substrate. Further support for operating in this dilution regime is gained from looking at transistor performance.

Fig. 3(f) shows transfer characteristics obtained from the four networks in Fig. 3(a–d). At the lowest concentration, good transistor performance is found with good current/mobility combined with good On/Off ratios: 3.1 $cm^2$/Vs and $>10^3$, respectively. Higher numbers have been found on other devices with mobility in the 10–20 $cm^2$/Vs range with On/Off $>10^4$ (Fig. 1(c)). For the sample set in Fig. 3, better mobility numbers would have been obtained with a slightly longer deposition time.

The experiment in Fig. 3 highlights the critical importance of concentration on network morphology and transistor performance. From the highest dilution, increasing nanotube concentration does not impact performance so strongly: going from 0.9 μg/mL to 2.2 μg/mL leads to some reduction in mobility with similar On/Off ratio. In those networks, nanotubes are not significantly bundled; otherwise mobility in excess of 10 $cm^2$/Vs with good On/Off ratio would not be possible (as shown in Fig. 1(c)). As the concentration increases further, the nanotube network becomes patchier and consequently contains a decreasing number of active pathways for current flow. The gate is still quite effective at modulating current: The network is still largely interconnected with individual SWCNTs and bundles present in the network do not produce percolating paths by themselves. As the concentration increases further to 5.6 and 14.1 μg/mL, transistor performance degrades substantially with a weak current modulation seen in the gate sweeps. Patches containing an increasing number of nanotubes become the dominant path for conduction. SEM in Fig. 3(d) shows that significant patch overlap exists and individual nanotube junctions appear in small number. Transport in nanotubes coalesced during droplet evaporation (micro-coffee stain) is similar to devices made of bundles where reduced gate action is observed [29,30]. We should highlight that even with twice the amount of SWCNTs, the 14.1 μg/mL film does not match the current carrying capacity of the 0.9 μg/mL film, which is on average sparser but presents much greater uniformity. These samples will be characterized further to obtain distributions of bundle size using an AFM based protocol [31].

### 3.3. Maskless patterning

We would like to address an essential requirement for deposition methods in printed electronics: patternability. Aerosol processes are very much compatible with shadow masking and one example is shown in Fig. S8. The small size of droplets combined with efficient solvent evaporation produces patterns with little material being drawn under the mask. With current technology in mask fabrication, feature sizes down to 10 μm are fairly

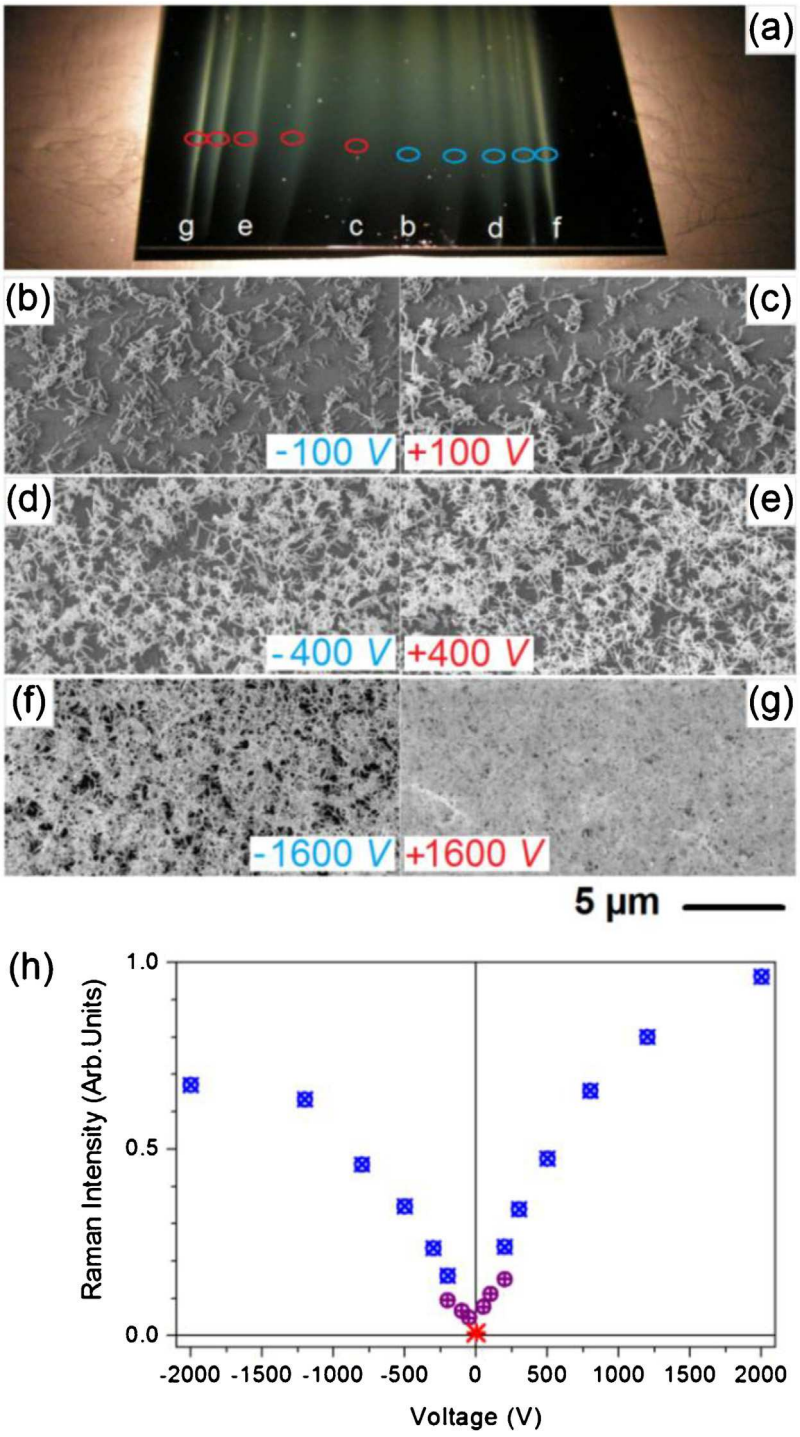


**Fig. 2.** Carbon nanotube thin films by droplet precipitation. (a) Macro-photography of $SiO_2$/Si substrates with carbon nanotube thin films deposited under increasing voltages using a nozzle with a slit aperture. Between each condition, the sample is translated laterally to obtain non-overlapping deposits. Sample size is about 22 × 28 $mm^2$. Colored circles correspond to approximate location for electron microscopy images in (b) to (g). (b)-(g) Scanning electron microscopy images taken from films deposited at different voltages. A complete set of images is shown in Fig. S4. Solution concentration was 3 µg/mL. and deposition time, 60 s. (h) Amount of deposited SWCNT determined by G-band Raman intensity as a function of applied voltage. Macro-photography of the samples is shown in Fig. S5.

realistic. Although this can prove useful in proof of concept studies, it is technologically more viable to have a process capable of producing patterns in a maskless fashion. Fig. 4 shows three examples of how this is possible by engineering both the gas flow and the electrostatic field.

Fig. 4(a) demonstrates how tightly the electrostatic field can focus the material. Optically, stripes deposited at the highest voltages appear very crisp with dimensions well under a millimeter. Fig. 4(b) presents a Raman intensity profile taken across a stripe and reveals a FWHM (Full-width at half-maximum) of 100 µm. Even with the overspread of material beyond 200 µm, we can safely say that transistors with channel width below 150 µm can be fabricated using this simple slit-shape nozzle. Patterning in the transverse direction can also be achieved by using a nozzle comprising multiple holes. An example of such a deposition is shown in Fig. 4(c). Individual islands of material as well as lines can be obtained with

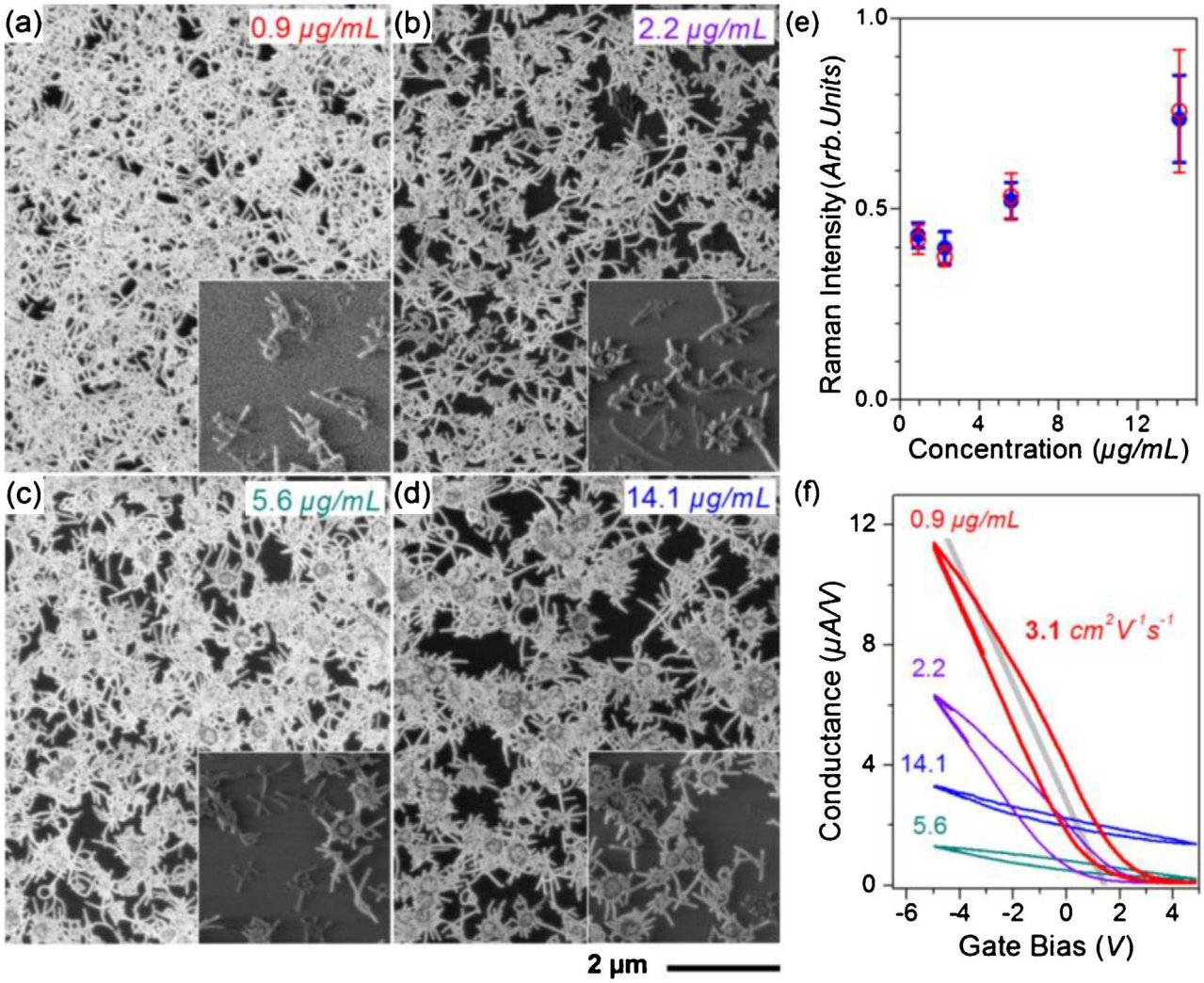


**Fig. 3.** Effect of solution concentration on carbon nanotube thin film morphology and device performance. Macro-photography pictures of the sample are shown in Fig. S6. Deposition was performed at 1600 V. (a–b) Scanning electron microscopy images of films obtained from carbon nanotube solutions of increasing concentration. Main images are taken from areas with highest coverage while inset images are taken from low coverage areas. The duration of the deposition was adjusted to obtain nominally the same amount material (75, 30, 12 and 4.8 s, respectively). (e) Amount of carbon nanotube deposited (using Raman G-band intensity) as a function of solution concentration for two sets of durations (75, 30, 12 and 4.8 s, and 50, 20, 8 and 3.2 s). Each data point is obtained from averaging Raman spectral intensities from 24 neighboring locations. The error bar represents one standard deviation and is a measure of thin film uniformity. (f) Device performance data obtained from films in (a)–(d). Forward and reverse gate sweeps are shown (12 μA/V is equivalent to 0.05 μA/μm for these devices). For the 0.9 μg/mL, a mobility 3.1 $cm^2$/Vs is calculated from the linear portion of the transfer curve (light gray). An ON/Off ration in excess of $10^3$ was obtained for this specific device. The substrate was $SiO_2$/Si (100 nm oxide); the channel length and width were 12 and 220 μm, respectively.

dimensions of order 500 μm. Here, in addition to the focusing action of the electrostatic field, the absence of flow mixing inherent to the laminar flow regime prevents material from depositing in areas between the holes. Improvements in nozzle design and flow engineering should allow feature sizes of 100 μm or less in both lateral and transverse directions. Another example of laminar flow deposition is shown in Fig. S9-10. In particular, Fig. S10 shows deposition using much finer masks fabricated using a photoetching process (Tecan, UK). With the 100 μm holes and 140 holes per inch line density (180 μm period), limited cross talk between neighboring deposits was observed. SEM images revealed excellent spatial selectivity with very few carbon nanotubes between deposits (Fig. S10(b–d)). This result indicates a potential for line densities of 300 *per inch*, a reference in printing technology.

A very appealing perspective for maskless patterning is through electric field engineering. In the previous examples, the electric field remained minimally patterned. However, we can possibly attribute the focusing of material to the nozzle curvature and/or to apertures (slit or holes). Going beyond the nozzle, we have performed a few initial tests as proof-of-concepts and demonstrated that upon patterning the ground electrodes, deposition of nanotubes occurs at specific locations. Fig. 4(d) shows one example of carbon nanotube islands deposited on a thin nylon film. During deposition, the nylon film was resting over the mask (see Fig. S11), a Teflon slab with copper wire inclusions connected to ground. Even if this experiment used a slit-shape nozzle with uniform delivery of droplets, deposition occurred mainly over the copper areas. This is a simple consequence of the higher field (and/or field gradient) in those areas compared to the support material (Teflon) where the ground is (spatially) approximately 2 mm lower.

## 4. Mechanism

It is in principle quite trivial to determine the mechanism leading to droplet precipitation, either from electro- (EP) or dielectrophoresis (DEP) [32]. In the former, mass transport occurs if

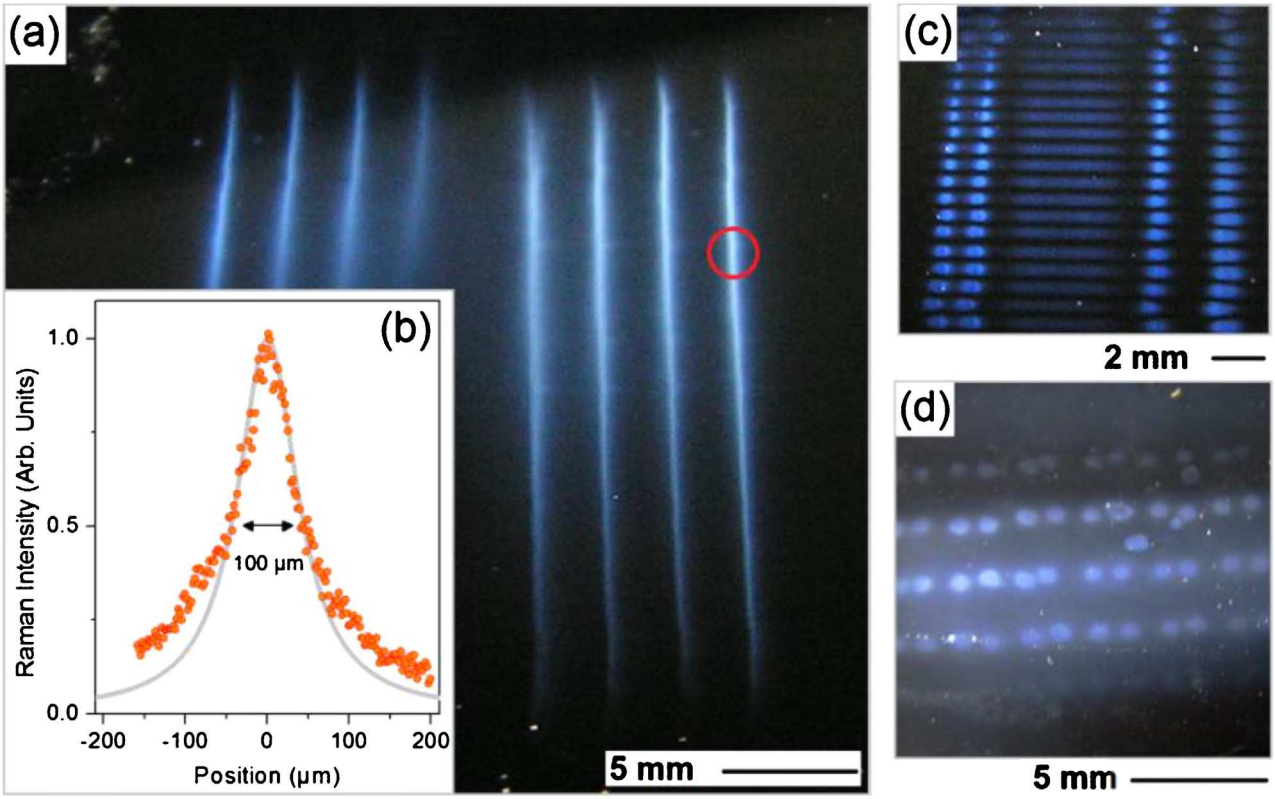


**Fig. 4.** Maskless deposition of carbon nanotube films. (a) Deposition from a slit-shape nozzle similar to Figs. 1–3. (b) Raman intensity profile across a stripe (red circle) of carbon nanotube material. The light gray line is a lorentzian profile. (c) Deposition pattern obtained from a nozzle with multiple apertures. From left to right, the sample is immobile for two durations and then continuously translated for 3 *mm*, and then immobile again for two more steps. (d) Deposition of carbon nanotubes on a nylon film using a sample holder with a patterned ground. More details on patterned deposition are presented in Fig. S8–S11.

droplets accumulate electrical charges upon their creation in the ultrasonic generator. The symmetry in the deposition between positive and negative voltages leads us to conclude that both positively and negatively charged droplets are present, in equal amounts. Given this symmetry, it might appear that DEP forces are responsible for droplet precipitation. In this case, droplets do not require holding a charge. However, sufficient electrical polarizability coupled with a field gradient is necessary. Our electrode geometry however does not seem to support the required field gradient. In order to completely exclude one of the two processes, we performed a deposition under an AC rather than DC voltage. A common approach in EP and DEP, the action of a time oscillating force averages to zero for charged droplets (EP) while for dipoles (DEP), a finite magnitude is expected from the quadratic dependence on the field. Fig. 5 shows the results of AC deposition performed at increasing frequencies (square wave modulation): At low frequencies below a few *Hz*, efficient deposition occurs with an amount of material similar to a DC deposition. As the frequency increases above 8 Hz, substantial reduction of deposited material is seen while above 30 Hz, essentially no material is visible. That result strongly supports electrophoresis. If dielectrophoresis was an important contribution to the process, material deposition would be seen at all frequencies. The frequency cutoff for electrophoresis represents a measure of how quickly droplets are attracted to the surface, of order of 100 ms. For an estimated flow rate of 1 cm/s, that corresponds to a 1 mm distance, of order of the gap between the nozzle and the sample.

In the present experiment, up to 2000 V was applied across a 2 mm gap, producing a field in excess of 1 MV/m. For a droplet carrying a single charge, the calculated force is 0.16 pN which seems like a small number. However, at a flow rate of 1 cm/s, we estimate

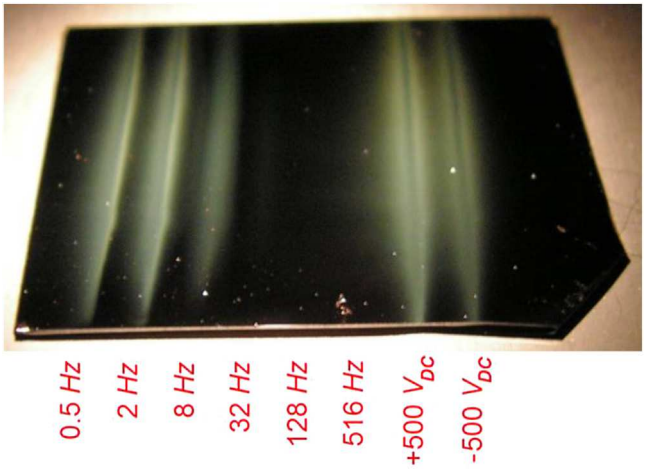


**Fig. 5.** Mechanism of droplet precipitation. Aerosol deposition performed under alternating voltage (500 V amplitude) at various frequencies (0.5–516 Hz) is compared with deposition at constant voltage. Concentration and duration were 2 µg/mL and 90 s, respectively. Sample dimension is 25×30 mm$^2$, approximately.

at 0.18 pN the force required to deflect a 1 µm droplet at the substrate boundary (see Supporting Information under "FORCES on a DROPLET"). The similarity between the two numbers is quite striking: However, it should only be seen as indicative that only few charges need to accumulate on a droplet to efficiently perturb its trajectory.

In Ref. [33], electrostatic precipitation was applied in a CVD (chemical vapor deposition) synthesis process to collect carbon nanotubes directly from the reactor. It was found that fields of order

100 kV/m were sufficient to maximize the collection yield of nanotubes holding on average 4 unit charges. Here, the higher fields reported can be attributed partly to the greater mass of droplets compared to free nanotubes, of course if the charge state is comparable. In the present method, the mechanism of charge generation and the role played by carbon nanotubes is not known.

## 5. Conclusion

We described an aerosol process that uses droplet electrophoresis for carbon nanotube deposition. Electrostatic forces generated on spontaneously charged droplets are sufficiently important to draw nanotubes towards a target substrate, even when the droplets are loaded with one or a few carbon nanotubes. sc-SWCNT assembled into networks on $SiO_2$/Si showed good performance in terms of mobility and On/Off ratio. Centimeter square areas can be covered in minutes, producing uniform films on the most difficult surfaces: [27] Carbon nanotube networks were assembled on six different polymer dielectrics and transistors in bottom gate configuration showed similar performance to $SiO_2$/Si, however, often with little to no gate hysteresis. Other than encapsulation and top gating, this aerosol method offers an alternative route to hysteresis free devices, and possibly improved performance for nanotube based gas sensors.

Currently, the printing throughput for transistor is estimated at $\approx 100\,s^{-1}$ and a thousand to million fold increase should be within reach. That would qualify the method in the medium throughput category. Patterning of carbon nanotube films is demonstrated using a shadow mask. More importantly for printed electronics, both gas flow and electric field can be engineered to produce patterns in a maskless fashion. Similar to electrospray, conformal deposition on 3D surfaces appears realistic. The method has the potential to provide an alternative path to a fully printed, fully additive process with several unique attributes.

## Acknowledgements

This work was performed within the Materials Thrust of the Printable Electronics program, under the dynamic leadership of Dr. P.R.L. Malenfant. Special thanks go to J. McKee for his help machining several components in this project, P. Finnie for some of the Raman data, J. Lapointe for SEM training, L. Chen for metal evaporation and N. Du for polymer dielectrics.

## Appendix A. Supplementary data

Supplementary data associated with this article can be found, in the online version, at http://dx.doi.org/10.1016/j.mtcomm.2017.01.002.

## References

[1] M. Shiraishi, T. Takenobu, T. Iwai, Y. Iwasa, H. Kataura, M. Ata, Chem. Phys. Lett. 39 (2004) 110–113.
[2] L. Hu, D.S. Hecht, G. Grüner, Nano Lett. 4 (2004) 2513–2517.
[3] S. Park, M. Vosguerichian, Z. Bao, Nanoscale 2013 (1727) 5.
[4] K. Higuchi, S. Kishimoto, Y. Nakajima, T. Tomura, M. Takesue, K. Hata, E.I. Kauppinen, Y. Ohno, Appl. Phys. Express 6 (2013) 085101.
[5] M.A. Meitl, Y. Zhou, A. Gaur, S. Jeon, M.L. Usrey, M.S. Strano, J.A. Rogers, Nano Lett. 4 (2004) 1643–1647.
[6] Q. Cao, S.-j. Han, G.S. Tulevski, Y. Zhu, D.D. Lu, W. Haensch, Nat. Nanotechnol. 8 (2013) 180–186.
[7] Q. Cao, S.-j. Han, G.S. Tulevski, Nat. Commun. 5 (2014) 5071.
[8] T. Toda, H. Frusawa, M. Furuta, Jpn. J. Appl. Phys. 52 (2013) 03BB09.
[9] S. Fujii, T. Tanaka, H. Suga, Y. Naitoh, T. Minari, K. Tsukagoshi, H. Kataura, Phys. Status Solidi B 247 (2010) 2750–2753.
[10] R.C. Tenent, T.M. Barnes, J.D. Bergeson, A.J. Ferguson, B. To, L.M. Gedvilas, M.J. Heben, J.L. Blackburn, Adv. Mater. 21 (2009) 3210–3216.
[11] S.L. Guillot, K.S. Mistry, A.D. Avery, J. Richard, A.-M. Dowgiallo, P.F. Ndione, J. van de Lagemaat, M.O. Reeseb, J.L. Blackburn, Nanoscale 7 (2015) 6556.
[12] M. Jeong, K. Lee, E. Choi, A. Kim, S.-B. Lee, Nanotechnology 23 (2012) 505203.
[13] A. Falco, L. Cina, G. Scarpa, P. Lugli, A. Abdellah, ACS Appl. Mater. Interfaces 6 (2014) 10593–10601.
[14] P. Beecher, P. Servati, A. Rozhin, A. Colli, V. Scardaci, S. Pisana, T. Hasan, A.J. Flewitt, J. Robertson, G.W. Hsieh, F.M. Li, A. Nathan, A.C. Ferrari, W.I. Milne, J. Appl. Phys. 102 (2007) 043710.
[15] T. Takenobu, N. Miura, S.-Y. Lu, H. Okimoto, T. Asano, M. Shiraishi, Y. Iwasa, Appl. Phys. Express 2 (2009) 025005.
[16] Y. Nobusa, Y. Takagi, S. Gocho, S. Matsuzaki, K. Yanagi, T. Takenobu, Jpn. J. Appl. Phys. 51 (2012) 06FD15.
[17] M. Ha, J.-W.T. Seo, P.L. Prabhumirashi, W. Zhang, M.L. Geier, M.J. Renn, C.H. Kim, M.C. Hersam, C.D. Frisbie, Nano Lett. 13 (2013) 954–960.
[18] S.G. Bucella, J.M. Salazar-Rios, V. Derenskyi, M. Fritsch, U. Scherf, M.A. Loi, M. Caironi, Adv. Electron. Mater. (2016), http://dx.doi.org/10.1002/aelm.201600094.
[19] C.M. Homenick, R. James, G.P. Lopinski, J. Dunford, J. Sun, H. Park, Y. Jung, G. Cho, P.R.L. Malenfant, ACS Appl. Mater. Interfaces 8 (2016) 27900–27910.
[20] J. Ding, Z. Li, J. Lefebvre, F. Cheng, G. Dubey, S. Zou, P. Finnie, A. Hrdina, L. Scoles, G.P. Lopinski, C.T. Kingston, B. Simard, P.R.L. Malenfant, Nanoscale 6 (2014) 2328.
[21] J. Ding, Z. Li, J. Lefebvre, F. Cheng, J.L. Dunford, P.R.L. Malenfant, J. Humes, J. Kroeger, Nanoscale 7 (2015) 15741.
[22] Z. Li, J. Ding, P. Finnie, J. Lefebvre, F. Cheng, C.T. Kingston, P.R.L. Malenfant, Nano Res. 8 (2015) 2179.
[23] P. Finnie, J. Ding, Z. Li, C.T. Kingston, J. Phys. Chem. C 118 (2014) 30127.
[24] Z. Li, J. Ding, J. Lefebvre, P.R.L. Malenfant, Org. Electron. 26 (2015) 15.
[25] http://www.sonaer.com/241T_V.PDF.
[26] P. Kulkarni, G.J. Deye, P.A. Baron, J. Aerosol Sci. 40 (2009) 164–179.
[27] J. Lefebvre, J. Ding, Z. Li, F. Cheng, N. Du, P.R.L. Malenfant, Appl. Phys. Lett. 107 (2015) 243301.
[28] Z. Liu, J. Zhao, W. Xu, L. Qian, S. Nie, Z. Cui, ACS Appl. Mater. Interfaces 6 (2014) 9997.
[29] L. Hu, D.S. Hecht, G. Grüner, Nano Lett. 4 (2004) 2513–2517.
[30] T. Kim, G. Kim, W.I. Choi, Y.-K. Kwon, J.-M. Zuo, Appl. Phys. Lett. 96 (2010) 173107.
[31] D. Vobornik, S. Zou, G.P. Lopinski, Langmuir 32 (2016) 8735–8742.
[32] J. Voldman, Annu. Rev. Biomed. Eng. 8 (2006) 425–454.
[33] M.Y. Zavodchikova, T. Kulmala, A.G. Nasibulin, V. Ermolov, S. Franssila, K. Grigoras, E.I. Kauppinen, Nanotechnology 20 (2009) 085201.